metals

MDPI

Article

Mechanical Properties and the Microstructure of β Ti-35Nb-10Ta-*x*Fe Alloys Obtained by Powder Metallurgy for Biomedical Applications

Angélica Amigó [1], Angel Vicente [1], Conrado R. M. Afonso [2] and Vicente Amigó [1,*]

[1] Universitat Politècnica de València (UPV), Institut de Tecnologia de Materials (ITM), Camí de Vera s/n, 46022 Valencia, Spain; anamma@upvnet.upv.es (A.A.); avicente@mcm.upv.es (A.V.)

[2] Universidade Federal de São Carlos (UFSCar), Departamento de Engenharia de Materiais (DEMa), Rodovia Washington Luis, km 235, CEP 13565-905 São Carlos, SP, Brazil; conrado@ufscar.br

* Correspondence: vamigo@upvnet.upv.es; Tel.: +34-963-877-623

Received: 3 December 2018; Accepted: 12 January 2019; Published: 12 January 2019

Abstract: Titanium alloys with high refractory metals content are required to obtain advanced biomaterials with a low elastic modulus and good mechanical properties. This work studies the influence of Fe content on the microstructure and mechanical properties of powder metallurgy Ti35Nb10Ta(Fe) alloys, with Fe content additions of 1.5, 3.0 and 4.5 wt%. Samples are obtained by uniaxial compaction and sintering at 1250 °C and 1300 °C. Microstructural characterization is performed by scanning and transmission electron microscopy and mechanical characterization by bending, compression and a hardness test. The elastic modulus is measured by the ultrasounds technique. The results show a 10% increase in the maximum bending strength with an increase in the sintering temperature. The obtained microstructure is composed of β-Ti phase (bcc) and some regions where laths of the α-Ti (hcp) phase occur along the grain boundaries. Fe addition slightly improves the stability of the β-Ti phase and conversely decreases the maximum strength and final deformability due to increased porosity. The Ti35Nb10Ta alloy composition displays better properties, with an elastic modulus of 75 GPa, a bending strength of 853 MPa and compression strength of 1000 MPa.

Keywords: β titanium alloys; anelastic relaxation; elastic modulus; phase transformation

1. Introduction

Metallic biomaterials, such as stainless steels, Co-Cr alloys, commercially pure titanium (c.p. Ti) and Ti alloys, are extensively employed. Titanium presents two different allotropic phases; the β phase (bcc) in Ti alloys exhibits a significantly lower elastic modulus than the equilibrium α-Ti (hcp) phase [1]. Studying β-Ti alloys is interesting due to their higher corrosion resistance and lower elastic modulus [2,3]. These alloys also present good biocompatibility and use low-toxicity elements to obtain materials, excluding elements such as Al or V, which are related with some clinical problems [4,5]. To stabilize the β-Ti phase, increased contents of refractory elements, such as Nb, Ta and Mo, are commonly used. These isomorphous β-stabilizer elements present very good biocompatibility that is suitable for applications such as biomaterials [6] and can present favourable mechanical properties with a low elastic modulus. These properties can be changed by thermomechanical processing due to α″ precipitation and α transformation during aging [7]. Ti-Nb-base alloys are promising materials for biomedical applications given the properties they exhibit. These alloys can show different structures depending on composition and thermomechanical processing [8]. The addition of Ta to Ti-Nb alloys provides better biocompatibility and improved corrosion resistance [9].

The other β-stabilizer element types that can be added to obtain β-Ti phase stability are the eutectoid types: Fe, Cr, Co or Mn [10]. These elements have a stronger effect on β-Ti phase stabilization

but result in less biocompatibility. The addition of small percentages of these elements can enhance β-Ti stability and lower the cost of the material.

Fe has a critical content for retaining a 100% β-Ti phase. This value is 3.5 wt% in the Ti-Fe alloy system under quenching conditions [11]. Based on the molybdenum equivalent, Fe presents a stronger β-Ti phase stabilization effect [10]. As these low Fe contents more strongly affect β-Ti (bcc) phase stabilization [12], the solubility of Fe in β-Ti (both bcc structures) causes simple solution strengthening, while additions above 2 wt% Fe significantly increase strength [13]. However, the significant biocompatibility of the different alloys containing Fe has been reported in numerous studies and does not sacrifice the biochemical suitability of alloys [13–15].

The principal difficulty in these alloy types is the manufacturing process. In this case, powder metallurgy can provide good process technology to create customized materials but with its own limitations, such as porosity, lack of diffusion and increased grain size with different sintering parameters [16]. To obtain materials using powder metallurgy, the use of stronger β-Ti stabilization elements can provide better phase distribution, with less content in the α-Ti phase. This offers the possibility of decreasing the employed refractory to improve the diffusion problems that occur during the manufacturing process when refractory character elements are used.

The objective of this work is to study the influence of Fe content using two sintering temperatures in the microstructure and mechanical properties of Ti35Nb10TaxFe (x = 1.5, 3.0 and 4.5 wt% Fe) β-Ti alloys obtained by conventional powder metallurgy.

2. Materials and Methods

The powder metallurgy of elemental blended powders was used to obtain alloys. The nominal compositions of β-Ti were: Ti35Nb10Ta, Ti35Nb10Ta1.5Fe, Ti35Nb10Ta3Fe and Ti35Nb10Ta4.5Fe (wt%). The commercially irregular pure metal powders were supplied by Atlantic Equipment Engineers (Upper Saddle River, NJ, USA) with high purity and in different sizes: Ti (99.7% pure, 55 μm median diameter), Nb (99.8%, 20 μm), Ta (99.8%, 8 μm) and Fe (99.9%, 34 μm). Blending of powders was conducted in an inversing mixer (Inversina 2L, BioEngineering AG., Wald, Switzerland) at 50 rpm for 30 min. Compaction was done in a floating die of 30 × 12 mm and 10.5 g of blend powders to obtain an approximate thickness of 5 mm. A hydraulic press of 500 kN (Model 1343, INSTRON, Norwood, MA, USA) was used to apply 600 MPa of uniaxial pressure. Sintering was performed at two temperatures, 1250 °C and 1300 °C, for 3 h in a high-vacuum ($<10^{-4}$ mbar) tubular furnace (Model 15-75-450, Carbolite Gero GmbH & Co., Neuhausen, Germany) with a cooling cycle in the furnace. The heating rate was 10 °C/min and the typical cooling rate inside the furnace was approximately 1.5 °C/min.

Transversal sections were prepared for metallography to study microstructure characterization. Samples were ground with SiC paper and polished using 9 μm diamond suspension and colloidal silica in a finishing step. Microstructure characterization was made with a field emission (FEG) scanning electron microscope (FESEM Ultra 55, Zeiss Oberkochen, Germany) using backscattered electrons (BSE) to reveal the microstructure and to obtain the grain size measurements and percentage of Nb particles that lacked diffusion by an image analysis. The SEM is equipped with an X-ray dispersive energy detector (EDS, Oxford Instruments, Abingdon, UK). X-ray diffraction (XRD) (CubicPro, Malvern Panalytical, Almelo, The Netherlands) was used to determine the phases in samples. The Rietveld method provides the volume fraction of the different phases obtained in the XRD results. Selected specimens were also investigated by (scanning) transmission electron microscopy (TEM/STEM) with a FEI Tecnai F20 G2 (Thermo Fisher Scientific, Waltham, MA, USA) at 200 kV and a field emission gun (FEG) coupled with an EDAX EDS detector. Oxygen was measured by the LECO 400 series equipment (LECO, Saint Joseph, MI, USA). Porosity was determined by an image analysis of the SEM micrographs (15 fields at the 100× magnification) using the IMAGE J software (Image J 1.50b, National Institutes of Health, Bethesda, MD, USA). Density was obtained by the Archimedes method.

Mechanical characterization was made by bending tests (Autograph AG100, Shimadzu, Kyoto, Japan) according to ISO 3325:1996. Compression tests (5 samples each test) were conducted using the position control to apply the load and a limit of displacement of 2 mm was used. Measurements with the Vickers hardness test (Centaur Model HD-9-45) were taken using 10 kg applied for 15 s. The elastic modulus was measured by an ultrasonic test (Echograph Digital, Karl Deutsch GmbH, Wuppertal, Germany).

3. Results

The X-ray diffraction analysis for the Ti35Nb10TaxFe alloys for a sintering temperature of 1250 °C showed the presence of primarily the β-Ti phase, along with low-intensity peaks of the α-Ti phase (Figure 1). Similar results were obtained for the high sintering temperature, with lower intensity in the α-Ti peaks. The intensity of the α phase peaks (and volume fraction) lowered with Fe addition, which led to greater β phase stabilization under the same conditions as in the sintering process. The volume fraction (Table 1) of the α-Ti phase lowered from 8%, for Ti35Nb10Ta sintered at 1250 °C to 0% when 4.5% of Fe were added and also lowered to 4% for Ti35Nb10Ta with an increase in the sintering temperature (1300 °C).

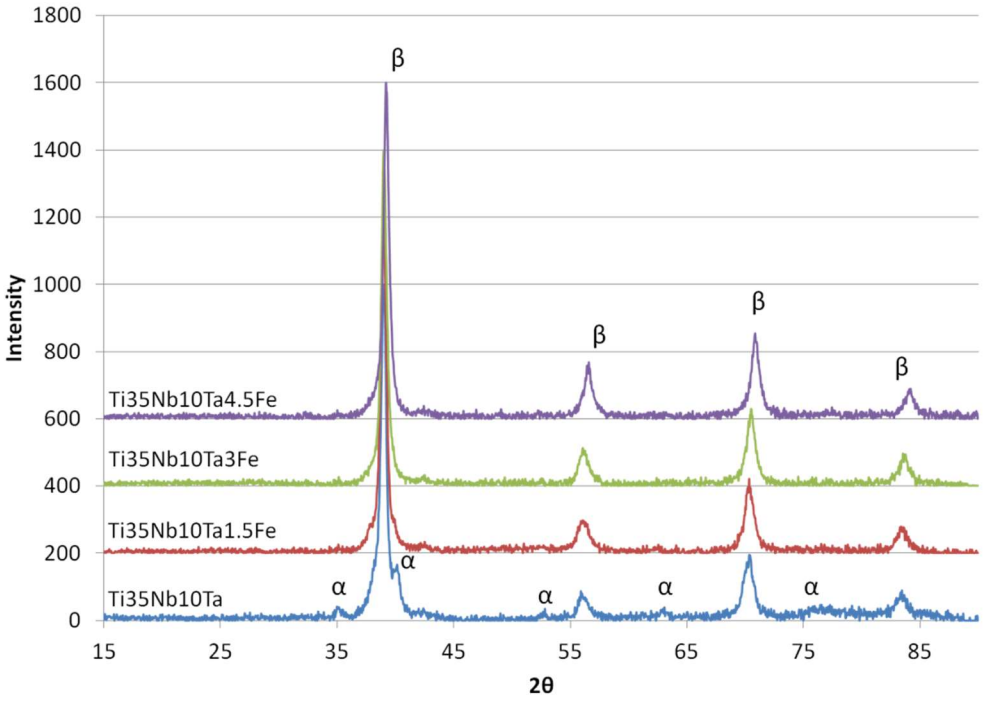

Figure 1. X-ray diffraction (XRD) patterns for compositions Ti35Nb10Ta, Ti35Nb10Ta1.5Fe, Ti35Nb10Ta3Fe and Ti35Nb10Ta4.5Fe sintered at 1250 °C.

The oxygen measurements for all the compositions gave a percentage of approximately 0.7%, with minimum variation among samples. By adding oxygen from 0.3% to 1.8%, Wei et al. [17] confirmed that no significant change took place from the stabilized β-Ti phase for TNZT alloys; therefore, the 0.7% oxygen fraction in the present work might not have caused significant changes in the microstructure and properties of Ti35Nb10Ta(xFe) alloys, in the same way as Wei et al. confirmed in their study.

Table 1. Volume fraction of the α-Ti phase obtained from XRD by the Rietveld method and percentage of Nb without diffusion.

Composition	1250 °C		1300 °C	
	% Alpha (±1%)	% Nb (±0.02%)	% Alpha (±1%)	% Nb (±0.02%)
Ti35Nb10Ta	8	2.63	4	2.70
Ti35Nb10Ta1.5Fe	5	1.31	1	1.15
Ti35Nb10Ta3Fe	2	1.18	0	0.51
Ti35Nb10Ta4.5Fe	0	1.07	0	0.45

Figure 2 presents the SEM images in the BSE signal of the Ti35Nb10Ta(3Fe) alloys sintered at 1250 °C, where lack of diffusion is observed primarily in Nb particles and possibly in Ta. The EDS analysis confirmed that some Nb-rich powder particles presented lack of diffusion and were still included in the microstructure. The percentage of Nb particles was obtained and showed a similar 2.7% content for the Ti35Nb10Ta alloy at both sintering temperatures. A small amount of added Fe decreased the Nb content without diffusing by 50% regardless of sintering temperature and with values of 1.2% for Ti35Nb10Ta1.5Fe. When 3.0% or 4.5% of Fe were used, the effect of the sintering temperature was greater as lack of diffusion of the Nb particles lowered from 1.1% to 0.5% at 1300 °C. Another observed factor was that porosity increased with Fe addition as some larger porous areas appeared (Figure 2b), which may be related to the size of the Fe powder particles used as the raw material in the P/M alloys [18]. The high diffusion ratio presented by Fe inside Ti would suffice enough sintering but it depends on Fe particle size. If a coarse particle size was used, the differences in the diffusion ratios provided the diffusion of Fe inside Ti but not Ti inside Fe and larger porous appeared, similarly to the porosity obtained by O'Flynn and Corbin in their studies [18].

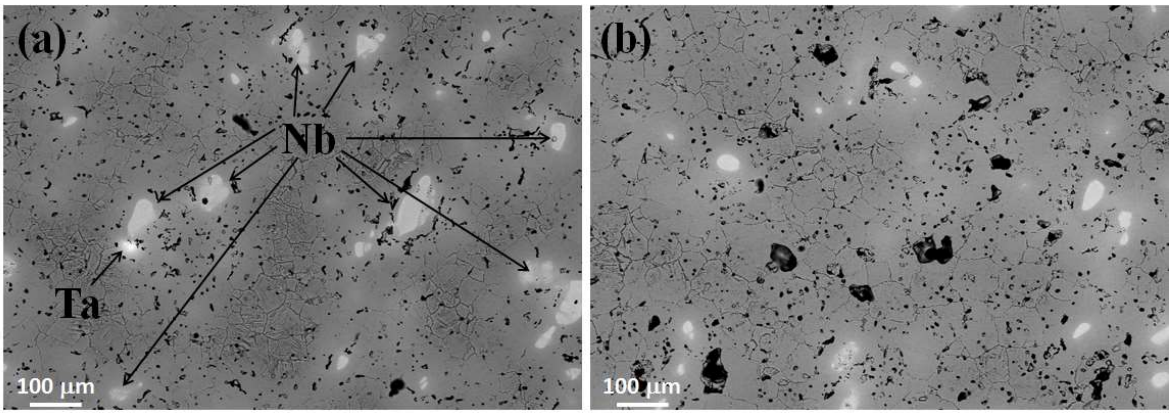

Figure 2. Backscattered electron images of (**a**) Ti35Nb10Ta and (**b**) Ti35Nb10Ta3Fe sintered at 1250 °C.

The microstructure of the Ti35Nb10TaxFe (x = 1.5, 3.0 and 4.5 wt% Fe) alloys sintered at 1250 °C and 1300 °C (Figure 3) illustrated some α + β zones, where the α-Ti phase appeared with a lath morphology precipitated on the grain boundary and inside the β-Ti grains. The regions surrounding the Nb particles (β-stabilizer-rich region) reached a stable β-Ti phase condition and even retained the β-Ti (bcc) structure at room temperature under the furnace cooling conditions [19]. Figure 3 shows the decreasing Nb particles, as reported in Table 1. When Fe addition increased, β-Ti phase stability slightly improved, which seemed to favour the diffusion of Nb and its dissolution into the β-Ti matrix by reducing the size and fraction of the Nb-rich particles. Higher sintering temperatures (1300 °C) and Fe addition led to a better diffusion of the refractory alloying elements. This scenario is depicted in Figure 3d–f, where the β-Ti phase presented better homogeneity and the α + β zones became smaller due to the better diffusion of the β-stabilizer elements.

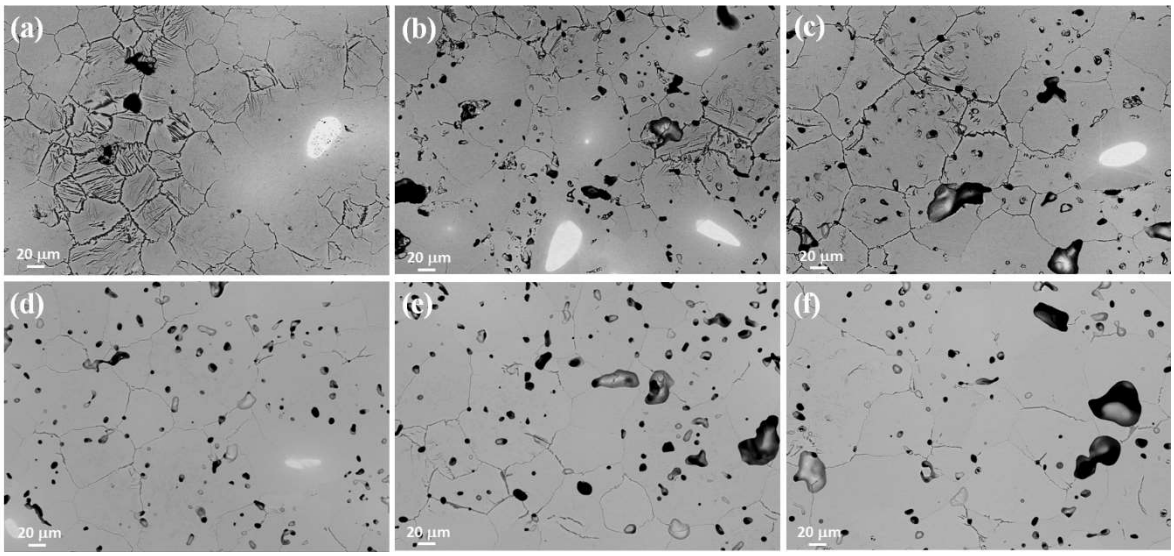

Figure 3. The scanning electron microscopy (SEM) images of the backscattered electron (BSE) signal of (**a**) Ti35Nb10Ta1.5Fe, (**b**) Ti35Nb10Ta3Fe (**c**) Ti35Nb10Ta4.5Fe sintered at 1250 °C and of (**d**) Ti35Nb10Ta1.5Fe, (**e**) Ti35Nb10Ta3Fe (**f**) Ti35Nb10Ta4.5Fe sintered at 1300 °C.

Figure 4 shows the EDX mapping results in the α + β region on the Ti35Nb10Ta1.5Fe sintered at 1250 °C. The α-Ti phase presents a lath morphology, where the amount of Ti identified by EDX mapping was bigger in this area than in the β phase regions. The Nb is concentrated in the β-phase regions, with the low content of niobium in the alpha phase laths. In these α-Ti laths, the amount of Fe and Ta was also lower, although the Ta and Fe distribution presented more homogeneity and the content inside the α-Ti phase slightly decreased. However, this lack of homogeneity may indicate that the microstructure is not in equilibrium due to the lack of diffusion of the refractory elements in the titanium.

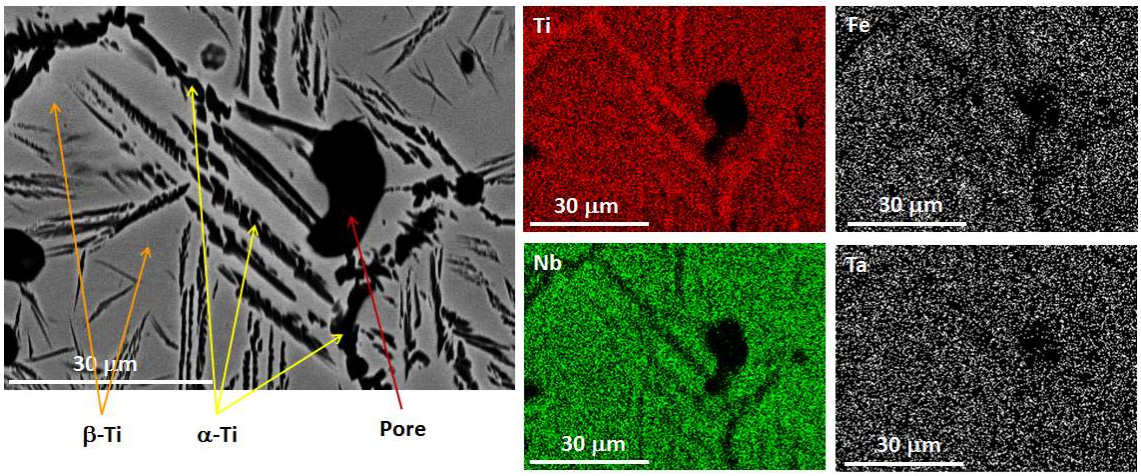

Figure 4. Selected EDX mapping of the α-Ti phase in the Ti35Nb10Ta1.5Fe alloy sintered at 1250 °C. The distribution of the different elements is indicated.

Figure 5 illustrates the TEM images in the bright field (BF) mode for the Ti35Nb10Ta alloy sintered at 1250 °C, where two regions are observed. The β-stabilizer poor region (α + β zone) is shown in Figure 5a and the β-Ti region (β-stabilizer rich) with the nanometric ω phase is illustrated in Figure 5b. The selected area diffraction patterns (SADP) in Figure 5c show the respective orientation relationships between the α/β phases on the zone axis [0001]α//[110]β and in Figure 5d for the orientation relationships between the β/ω phases: $[11\bar{2}0]\omega//[1\bar{1}0]\beta$. The main reason why the ω phase

was not detected by the XRD analysis was because of a smaller volume fraction, whose small size means it is impossible to be detected by this technique. An isothermal metastable ω phase (hcp) was formed at the slow cooling rate in the furnace after the sintering process. In this case, it was not possible to associate it with an athermal ω phase, which is typical of the water-quenched samples from the β-Ti phase field [19].

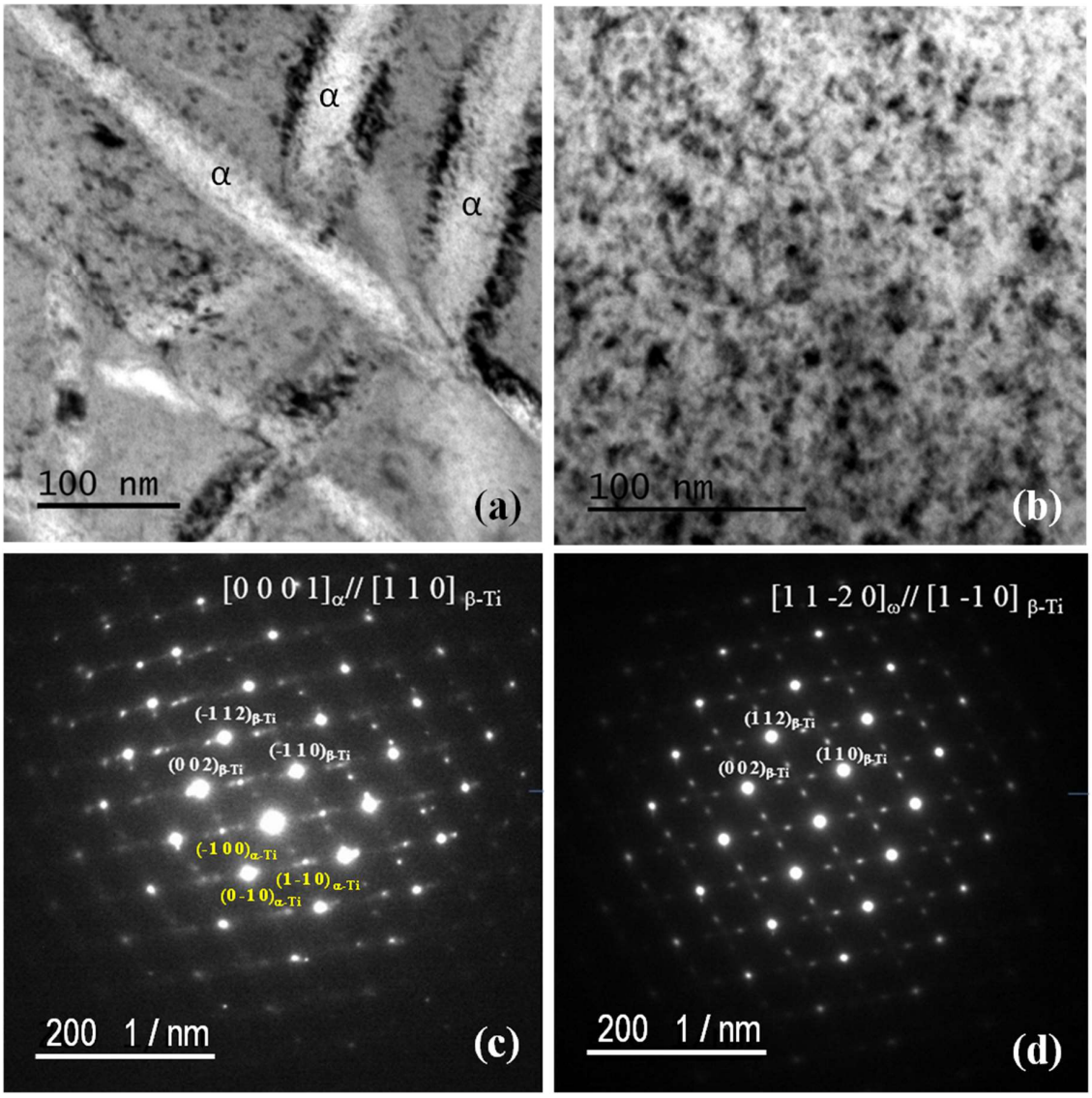

Figure 5. The transmission electron microscopy (TEM) images in the bright field (BF) mode for the Ti35Nb10Ta alloy sintered at 1250 °C, (**a**) the α + β zone and (**b**) the β-Ti region with the nanometric ω phase, followed by respective selected area diffraction patterns (SADP) showing (**c**) the zone axis [0001]α//[110]β and (**d**) $[11\bar{2}0]\omega//[1\bar{1}0]\beta$.

The grain size measurements reveal a significant increase with Fe addition, from 45 to 67 μm, according to the results in Table 2. This may be related to the effect of Fe on the stability of the β-Ti phase, which presents a larger grain growth at the process temperatures. For the samples sintered at 1300 °C, a larger grain size was obtained for the same compositions (Ti35Nb10Ta and Ti35Nb10Ta4.5Fe), which varied between 50 and 77 μm, respectively. Porosity has a similar effect with the addition of iron, which increases from 5.1% for the Ti35Nb10Ta alloy to 11.2% when 1.5% of Fe was added at 1250 °C. At 1300 °C, the same evolution is obtained with addition of Fe but at this temperature the porosity is slightly lower than at 1250 °C. But this small difference in porosity at both temperatures is defined by

the difference in open porosity that results from 0.8 to 2.1% for the sintering temperature of 1250 °C and 0.4 to 0.8% when sintering at 1300 °C. The closed porosity is practically the same for both sintering temperatures. Therefore, the experimental density followed the same pace as the porosity and this resulted in the β-titanium alloy density lowering from 5.70 g/cm^3 for Ti35Nb10Ta to 5.51 g/cm^3 when 4.5% by weight of Fe was added in the titanium alloy composition.

Table 2. Variation in porosity (%) and grain size (μm) with the composition of the Ti35Nb10TaxFe alloys and sintering temperatures.

Composition	% Porosity		Grain Size (μm)		Density (g/cm^3)	
	1250 °C	1300 °C	1250 °C	1300 °C	1250 °C	1300 °C
Ti35Nb10Ta	5.1 ± 0.6	4.2 ± 0.2	45 ± 2	50 ± 2	5.67 ± 0.01	5.70 ± 0.01
Ti35Nb10Ta1.5Fe	7.7 ± 0.6	6.4 ± 0.2	50 ± 1	62 ± 4	5.64 ± 0.02	5.63 ± 0.01
Ti35Nb10Ta3.0Fe	9.2 ± 0.3	8.3 ± 0.2	60 ± 2	69 ± 4	5.52 ± 0.02	5.56 ± 0.01
Ti35Nb10Ta4.5Fe	11.2 ± 0.2	10.2 ± 0.1	67 ± 1	77 ± 2	5.52 ± 0.07	5.51 ± 0.01

Table 3 shows the elastic modulus, E (GPa) and Vickers hardness (HV) for the Ti35Nb10TaxFe alloys at two sintering temperatures: 1250 °C and 1300 °C. Vickers microhardness remained constant, approximately 340 HV for all the compositions at both sintering temperatures. Fe addition brought about a slight increase in the elastic modulus, which rose from 75 to 83 GPa when 4.5 wt% of Fe was added. The elastic modulus showed a narrow variation range when the sintering temperature went higher, with an initial value of 76 GPa for Ti35Nb10Ta at 1300 °C and one of 81 GPa when 4.5% of Fe was added.

Table 3. The Elastic Modulus, E (GPa) and Vickers hardness (HV) for Ti35Nb10TaxFe alloys at sintering temperatures of 1250 and 1300 °C.

Composition	Hardness (HV 0.3)		Elastic Modulus (GPa)	
	1250 °C	1300 °C	1250 °C	1300 °C
Ti35Nb10Ta	341 ± 30	334 ± 28	75 ± 3	76 ± 1
Ti35Nb10Ta1.5Fe	338 ± 26	340 ± 25	79 ± 2	77 ± 1
Ti35Nb10Ta3.0Fe	340 ± 26	340 ± 33	81 ± 1	80 ± 1
Ti35Nb10Ta4.5Fe	345 ± 25	331 ± 39	83 ± 2	81 ± 1

To evaluate the mechanical properties, bending and compression strength (MPa) are reported in Table 4. The results show that bending strength decreased when the amount of Fe increased in the titanium alloy composition. Maximum strength improved for all Ti35Nb10TaxFe compositions when the maximum sintering temperature changed from 1250 to 1300 °C. However, compression strength remained constant, at approximately 1000 MPa for all the compositions at a sintering temperature of 1250 °C. Compression strength increased slightly for the same crosshead displacement, up to 1050 MPa, with an increase in the sintering temperature up to 1300 °C. Porosity and grain size (Table 2) both influenced the mechanical properties, primarily bending strength. Higher sintering temperatures reduced the alloy's porosity, with a slight increase in grain size. Both effects translated into high bending strength values.

Fe content was another factor that influenced the bending strength values. As the amount of Fe content increased, two effects changed in the titanium alloys: pore size increased and the amount of the α + β areas reduced. Based on the microstructure and the formed phases, Fe addition led to the β-Ti phase stabilization in the Ti35Nb10TaxFe alloys, diminished the fraction of the α + β zones in the microstructure and lowered the percentage of the α-Ti phase, according to the XRD patterns and microstructure characterization. As the α-Ti phase presented greater mechanical strength and hardness than the β-Ti phase without Fe, the Ti35Nb10Ta alloy showed the highest bending strength values for

both sintering temperatures. The bigger pores and larger amount of the β phase were translated into lower bending strength values when the amount of Fe increased in the Ti35Nb10Ta alloys.

Table 4. Mechanical properties, bending and compression strength (MPa) for the Ti35Nb10TaxFe alloys at sintering temperatures of 1250 °C and 1300 °C.

Composition	Bending Strength (MPa)		Compression Strength (MPa)	
	1250 °C	**1300 °C**	**1250 °C**	**1300 °C**
Ti35Nb10Ta	776 ± 45	853 ± 51	1000 ± 20	1067 ± 36
Ti35Nb10Ta1.5Fe	669 ± 58	750 ± 59	974 ± 5	1059 ± 21
Ti35Nb10Ta3.0Fe	615 ± 26	700 ± 41	994 ± 8	1040 ± 5
Ti35Nb10Ta4.5Fe	544 ± 21	599 ± 14	1035 ± 6	1074 ± 9

4. Discussion

Nowadays, two main manufacturing methods are employed to obtain complex β-Ti alloys: casting [20,21] and powder metallurgy. Several authors have studied the use of complementary processes, such as hot-forging, plastic deformation [22] and heat treatments [23], to obtain the desired microstructure and mechanical properties.

In this paper, powder metallurgy methods were employed to obtain complex β-Ti alloys with different Fe additions. The microstructure obtained after conventional powder metallurgy processes was composed mainly of the β-Ti phase with some α-Ti phase in the grain boundaries. Inside the β grains in specific regions, the α + β regions were similar to those obtained by Santos et al. for Ti35Nb sintered at 1300 °C [24]. Fe addition reduced the quantity of the α-Ti phase as this element had a stronger beta stabilization effect and the obtained results were similar to those reported by Kopova et al. [13] in her study into beta titanium alloys for biomedical applications.

The high Nb and Ta contents led to lack of diffusion for the temperatures and times used to sinter alloys as these refractory elements present high melting temperatures and densities. Zhao et al. explained the diffusion process of Nb particles in the Ti matrix for the Ti16Nb alloy. The presence of Nb particles acts as a diffusion barrier and it is necessary to use high sintering temperatures to obtain good chemical homogeneity [25]. The thermal process involved in powder metallurgy, especially the cooling rate, may cause grain growth and α phase transformation on the grain boundary [16].

In the present study, better diffusion of Nb in the Ti matrix was achieved when the 1300 °C sintering temperature was employed. The use of higher sintering temperatures resulted in grain size growth and this effect was enhanced when Fe was added to the alloy composition. This resulted in a 10% grain size increment for Ti35Nb10Ta and one up to 24% when Fe was added to the titanium alloy composition. Fe addition decreased the α-Ti phase but a small fraction remained in the microstructure. The amount of Fe tested herein could not eliminate the α phase transformation on the grain boundary. Grain size presented a relationship with the volume fraction of the α-Ti phase. Figure 6 confirms the increasing grain size tendency when the contents in the α-Ti phase lowered, which blocked grain growth due to its precipitation on the grain boundaries [26]. Lopes et al. also reported an increased grain size with β-Ti phase stabilization [27].

The study of porosity for PM Ti35Nb10Ta alloys has shown that Fe addition affects both characteristics. O'Flynn and Corbin obtained similar results in their studies [18], as large pores were observed in the microstructure analysis when adding pure Fe powder (~34 μm) to the titanium alloy composition. One approach to reduce big porosity due to Fe addition, which acts as a stress concentration factor and reduces mechanical properties, would be to use a finer powder particle size (1–5 μm) than that employed herein (34 μm). The results showed that porosity increased linearly with incremented Fe content in the alloys' composition. Porosity showed an increase of 50% for Ti35Nb10Ta1.5Fe, 80% for Ti35Nb10Ta3Fe and 120% for Ti35Nb10Ta4.5Fe, compared with the Ti35Nb10Ta alloy at 1250 °C. However, it lowered and came close to 10% for the 1300 °C sintering temperature, as Figure 7 shows.

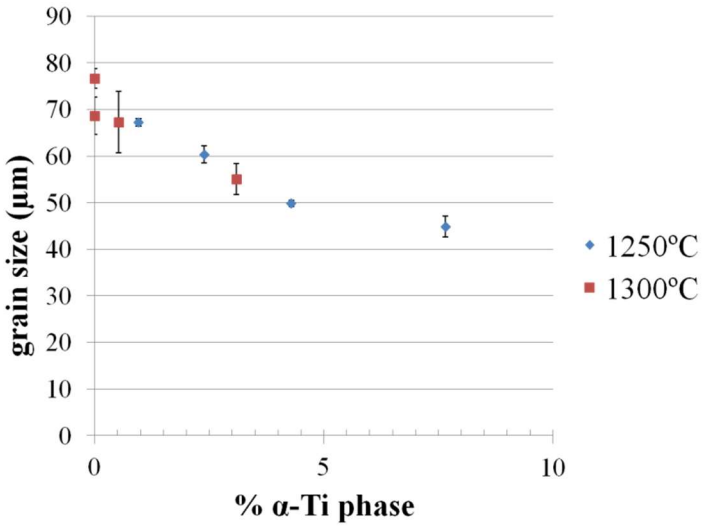

Figure 6. Relationship between the grain size and volume fraction of the α-Ti phase at 1250 and 1300 °C.

The presence of the metastable ω phase precipitated on the nanoscale and increased the elastic modulus and the Vickers microhardness of the β-Ti alloys [28–30]. This would explain the effect of Nb% on the precipitation temperature of the ω phase when samples were rapidly solidified. However, ω phase precipitates can act as α-Ti phase nucleation sites [28]. Kim et al. [31] obtained a decrease in the size and quantity of omega phase when adding Ta to Ti-Nb alloys, observing a decrease in the intensity of the omega phase in SADP, in the same way that is observed in this work when iron is added. On the other hand, Lin et al. reported how Fe addition can reduce the intensity of the ω phase peaks in XRD [32], which may be due to a reduced ω phase size [33]. Another factor that limits ω phase formation is the oxygen content ratio, which stabilizes the α-Ti phase and limits ω phase formation. Oxygen content brought about increased yield strength and reduced elongation [34]. Geng et al. reported a better relation between strength and ductility, which they obtained for a 0.7 wt% of O in the TNZT alloy [35]. The present study reports oxygen contents of 0.7% for all the compositions due to this the effect, which agrees with the results reported by other authors [17,35].

In other relevant works found in the literature [14,28], in where the authors have worked with arc melted, hot forged and quenched samples, an incremental change was obtained in the mechanical properties with Fe addition. Lee et al. obtained a maximum flexure strength of 1700MPa for the Ti25Nb7Fe cast alloy [36] and Lin et al. reported a tensile strength of 2450MPa for Ti7.5Mo2Fe [32]. However, the microstructure of this alloy was α + β, which provides higher strength than a complete β microstructure. Chaves et al. indicated a tensile strength of 520 MPa for the Ti19Zr10Nb1Fe cast alloy, which increased to 1050 MPa when rolled [14]. Bertrand et al. obtained 530MPa for tensile strength for a melted Ti25Nb25Ta alloy [37]. The values for the cast materials dropped to 544MPa, which was obtained for a Ti35Nb10Ta4.5Fe alloy sintered at 1250 °C. The reduction in maximum bending strength with Fe addition occurred with an increase in both the porosity and grain size of the Ti35Nb10TaxFe alloys. Figure 7 shows the linear tendency to an increasing bending strength when reducing both grain size and porosity. Higher sintering temperatures usually diminish porosity but increase grain size. The reduction in bending strength with Fe addition can be explained by increases in both porosity (%P) and grain size (µm). Grain size increased with better β-Ti phase stabilization and porosity as a wider size range of pure Fe powder was used (34 µm). The maximum strength values were 10% higher when a sintering temperature of 1300 °C was applied. However, strength dropped 30% when 4.5 wt% Fe was added to the Ti35Nb10Ta alloy, regardless of sintering temperature.

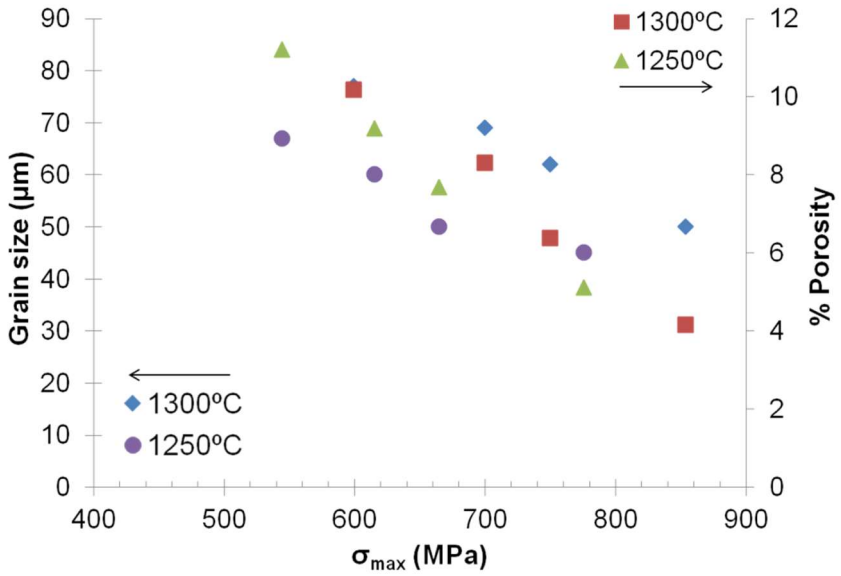

Figure 7. Relationship between flexural strength (σ) with grain size and porosity for 1250 °C and 1300 °C.

Chaves et al. indicated reductions in the elastic modulus and microhardness for the Ti(10-25)Nb3Fe alloy. The elastic modulus lowered from 72 to 65 GPa and microhardness from 479 to 289 HV, with increasing Nb content [28]. The reduction in both properties was caused by the increase in Nb contents, which obtained a β-Ti phase and a reduced ω phase. The microstructure changes of the Ti25Nb3Fe alloy due to deformation and heat treatment processes, which stabilize some α-Ti phases and decreased porosity, increased the elastic modulus to 79 GPa and microhardness to 300 HV. Zhang et al. reported an incremented elastic modulus when 1% of Fe was added to the Ti22Nb alloy [38], which corroborates the results of this work, where the elastic modulus increased with Fe additions in the Ti35Nb10Ta(xFe) alloys obtained by powder metallurgy.

5. Conclusions

The microstructure and mechanical properties of the Ti35Nb10TaxFe alloys (x = 1.5, 3.0 and 4.5 wt.%) obtained by powder metallurgy were studied for sintering temperatures of 1250 °C and 1300 °C. Based on the results, the following conclusions can be reached:

- The β-Ti phase was observed mainly with some residual α + β regions (β-stabilizer elements in lower concentrations) and greater β-Ti stabilization with Fe addition and sintering temperature. The nanometric ω phase was confirmed in the β-Ti phase by the TEM analysis.
- Porosity rose linearly with increasing Fe content. Adding 1.5% Fe to the alloy Ti35Nb gives an increase in porosity of 50%. When we add a greater amount of Fe, the increase is 20% compared to the previous alloy.
- Grain size increased with Fe additions and sintering temperature. β-Ti phase stabilization led to increments in grain size growth of 11%, 33% and 49% with 1.5%, 3% and 4.5% Fe additions compared with Ti35Nb10Ta; an increase between 11% and 24% was observed with sintering temperature.
- Bending strength decreased with Fe addition and followed a linear tendency, which diminished with increased porosity (%P) and grain size (µm). Fe addition brought about a slight increment between 5% and 10% in the elastic modulus (from E = 75 to 83 GPa). The compression strength (1000 MPa) and Vickers microhardness (340 HV) values remained constant for all the compositions.
- Fe addition did not prove interesting to obtain β-Ti alloys by powder metallurgy methods. Improved β-Ti stabilization was obtained but presented larger porosities due to Fe powders, which diminished the mechanical properties. The Ti35Nb10TaxFe alloy proved better with no Fe additions.

Author Contributions: A.A. and V.A. conceived and designed the experiments; Á.V. performed the mechanical experimentation; A.A. and C.R.M.A. made the microstructural characterization. All the authors analyzed the data. A.A. wrote the paper.

Funding: This research was funded by Universitat Politècnica de València Researcher Training Program, Spanish Ministry of Economy and Competitiveness grant number MAT2014-53764-C3-1-R, Generalitat Valenciana grant number PROMETEO/2016/040 and the European Commission with FEDER funds to purchase the research equipment.

Acknowledgments: The authors would like to thank the Electron Microscopy Service of the Universitat Politècnica de Valencia (UPV) and the Laboratório de Caracterização Estrutural (LCE) of DEMa-UFSCar.

Conflicts of Interest: The authors declare no conflict of interest.

References

1. Banerjee, R.; Nag, S.; Fraser, H.L. A novel combinatorial approach to the development of beta titanium alloys for orthopaedic implants. *Mater. Sci. Eng. C* **2005**, *25*, 282–289. [CrossRef]
2. Strietzel, R.; Hösch, A.; Kalbfleisch, H.; Buch, D. In vitro corrosión of titanium. *Biomaterials* **1998**, *19*, 1495–1499. [CrossRef]
3. Koike, M.; Fujii, H. The corrosion resistance of pure titanium in organic acids. *Biomaterials* **2001**, *22*, 2931–2936. [CrossRef]
4. Long, M.; Rack, H. Titanium alloys in total joint replacement—A materials science perspective. *Biomaterials* **1998**, *19*, 1621–1639. [CrossRef]
5. Gepreel, M.A.-H.; Niinomi, M. Biocompatibility of Ti-alloys for long-term implantation. *J. Mech. Behav. Biomed. Mater.* **2013**, *20*, 407–415. [CrossRef] [PubMed]
6. Geetha, M.; Singh, A.K.; Asokamani, R.; Gogia, A.K. Ti based biomaterials, the ultimate choice for orthopaedic implants—A review. *Prog. Mater. Sci.* **2009**, *54*, 397–425. [CrossRef]
7. Helth, A.; Pilz, S.; Kirsten, T.; Giebeler, L.; Freudenberger, J.; Calin, M.; Eckert, J.; Gebert, A. Effect of thermomechanical processing on the mechanical biofunctionality of a low modulus Ti-40Nb alloy. *J. Mech. Behav. Biomed. Mater.* **2017**, *65*, 137–150. [CrossRef]
8. Panigrahi, A.; Sulkowski, B.; Waitz, T.; Ozaltin, K.; Chrominski, W.; Pukenas, A.; Horky, J.; Lewandowska, M.; Skrotzki, W.; Zehetbauer, M. Mechanical properties, structural and texture evolution of biocompatible Ti–45Nb alloy processed by severe plastic deformation. *J. Mech. Behav. Biomed. Mater.* **2016**, *62*, 93–105. [CrossRef]
9. Karayan, A.I.; Park, S.; Lee, K.-M. Corrosion behavior of Ti-Ta-Nb alloys in simulated physiological media. *Mater. Lett.* **2008**, *62*, 1843–1845. [CrossRef]
10. Collings, E.W.; Boyer, R.; Welsch, G. *Materials Properties Handbook: Titanium Alloys*; ASM International: Materials Park, OH, USA, 1994.
11. Froes, F.H.S. *Titanium. Phisical Metallurgy Processing and Aplications*; ASM International: Materials Park, OH, USA, 2015.
12. Lopes, É.S.N.; Salvador, C.A.F.; Andrade, D.R.; Cremasco, A.; Campo, K.N.; Caram, R. Microstructure, Mechanical Properties and Electrochemical Behavior of Ti-Nb-Fe Alloys Applied as Biomaterials. *Metall. Mater. Trans. A Phys. Metall. Mater. Sci.* **2016**, *47*, 3213–3226. [CrossRef]
13. Kopova, I.; Stráský, J.; Harcuba, P.; Landa, M.; Janecek, M.; Bacákova, L. Newly developed Ti-Nb-Zr-Ta-Si-Fe biomedical beta titanium alloys with increased strength and enhanced biocompatibility. *Mater. Sci. Eng. C* **2016**, *60*, 230–238. [CrossRef] [PubMed]
14. Xue, P.; Li, Y.; Li, K.; Zhang, D.; Zhou, C. Superelasticity, corrosion resistance and biocompatibility of the Ti-19Zr-10Nb-1Fe alloy. *Mater. Sci. Eng. C* **2015**, *50*, 179–186. [CrossRef] [PubMed]
15. Biesiekierski, A.; Lin, J.; Li, Y.; Ping, D.; Yamabe-mitarai, Y.; Wen, C. Investigations into Ti-(Nb, Ta)-Fe alloys for biomedical applications. *Acta Biomater.* **2016**, *32*, 336–347. [CrossRef] [PubMed]
16. Teixeira, J.D.C.; Appolaire, B.; Aeby-Gautier, E.; Denis, S.; Bruneseaux, F. Modeling of the effect of the β phase deformation on the α phase precipitation in near-β titanium alloys. *Acta Mater.* **2006**, *54*, 4261–4271. [CrossRef]
17. Wei, L.S.; Kim, H.Y.; Miyazaki, S. Effects of oxygen concentration and phase stability on nano-domain structure and thermal expansion behavior of Ti–Nb–Zr–Ta–O alloys. *Acta Mater.* **2015**, *100*, 313–322. [CrossRef]

18. O'Flynn, J.; Corbin, S.F. The influence of iron powder size on pore formation, densification and homogenization during blended elemental sintering of Ti–2.5Fe. *J. Alloys Compd.* **2015**, *618*, 437–448. [CrossRef]
19. Tang, X.; Ahmed, T.; Rack, H.J. Phase transformations in Ti-Nb-Ta and Ti-Nb-Ta-Zr alloys. *J. Mater. Sci.* **2000**, *35*, 1805–1811. [CrossRef]
20. Lee, C.M.; Ju, C.P.; Lin, J.H.C. Structure-property relationship of cast Ti-Nb alloys. *J. Oral Rehabil.* **2002**, *29*, 314–322. [CrossRef]
21. Guo, S.; Zhang, J.; Cheng, X.; Zhao, X. A metastable β-type Ti–Nb binary alloy with low modulus and high strength. *J. Alloys Compd.* **2015**, *644*, 411–415. [CrossRef]
22. Yilmazer, H.; Niinomi, M.; Cho, K.; Nakai, M.; Hieda, J.; Sato, S.; Todaka, Y. Nanostructure of β-type titanium alloys through severe plastic deformation. *Adv. Mater. Lett.* **2014**, *5*, 378–383. [CrossRef]
23. Sakaguchi, N.; Niinomi, M.; Akahori, T.; Takeda, J.; Toda, H. Effect of Ta content on mechanical properties of Ti–30Nb–XTa–5Zr. *Mater. Sci. Eng. C* **2005**, *25*, 370–376. [CrossRef]
24. Dos Santos, D.R.; Henriques, V.A.R.; Cairo, C.A.A.; Pereira, M.D.S. Production of a low young modulus titanium alloy by powder metallurgy. *Mater. Res.* **2005**, *8*, 439–442. [CrossRef]
25. Zhao, D.; Chang, K.; Ebel, T.; Nie, H.; Willumeit, R.; Pyczak, F. Sintering behavior and mechanical properties of a metal injection molded Ti–Nb binary alloy as biomaterial. *J. Alloys Compd.* **2015**, *640*, 393–400. [CrossRef]
26. Málek, J.; Hnilica, F.; Veselý, J.; Smola, B. Heat treatment and mechanical properties of powder metallurgy processed Ti–35.5Nb–5.7Ta beta-titanium alloy. *Mater. Charact.* **2013**, *84*, 225–231. [CrossRef]
27. Lopes, E.S.N.; Contieri, R.J.; Button, S.T.; Caram, R. Femoral hip stem prosthesis made of graded elastic modulus metastable beta Ti Alloy. *Mater. Des.* **2015**, *69*, 30–36. [CrossRef]
28. Chaves, J.M.; Florêncio, O.; Silva, P.S., Jr.; Marques, P.W.B.; Afonso, C.R.M. Influence of phase transformations on dynamical elastic modulus and anelasticity of beta Ti-Nb-Fe alloys for biomedical applications. *J. Mech. Behav. Biomed. Mater.* **2015**, *46*, 184–196. [CrossRef] [PubMed]
29. Li, C.; Lee, D.; Mi, X.; Ye, W.; Hui, S.; Lee, Y. Phase transformation and age hardening behavior of new Ti-9.2Mo-2Fe alloy. *J. Alloys Compd.* **2013**, *549*, 152–157. [CrossRef]
30. Tane, M.; Nakano, T.; Kuramoto, S.; Niinomi, M.; Takesue, N.; Nakajima, H. Transformation in cold-worked Ti-Nb-Ta-Zr-O alloys with low body-centered cubic phase stability and its correlation with their elastic properties. *Acta Mater.* **2013**, *61*, 139–150. [CrossRef]
31. Kim, H.Y.; Hashimoto, S.; Kim, J.I.; Inamura, T.; Hosoda, H.; Miyazaki, S. Effect of Ta addition on shape memory behavior of Ti–22Nb alloy. *Mater. Sci. Eng. A* **2006**, *417*, 120–128. [CrossRef]
32. Lin, D.J.; Chern Lin, J.H.; Ju, C.P. Structure and properties of Ti–7.5Mo–xFe alloys. *Biomaterials* **2002**, *23*, 1723–1730. [CrossRef]
33. Hanada, S.; Izumi, O. Transmission electron microscopic observations of mechanical twinning in metastable beta titanium alloys. *Metall. Trans. A* **1986**, *17*, 1409–1420. [CrossRef]
34. Cho, K.; Niinomi, M.; Nakai, M.; Hieda, J.; Kanekiyo, R. Improvement of Tensile and Fatigue Properties of beta-Titanium Alloy while Maintaining Low Young's Modulus through Grain Refinement and Oxygen Addition. *Mater. Trans.* **2013**, *54*, 2000–2006. [CrossRef]
35. Geng, F.; Niinomi, M.; Nakai, M. Observation of yielding and strain hardening in a titanium alloy having high oxygen content. *Mater. Sci. Eng. A* **2011**, *528*, 5435–5445. [CrossRef]
36. Lee, C.M.; Ho, W.F.; Ju, C.P.; Chern Lin, J.H. Structure and properties of Titanium-25 Niobium-x iron alloys. *J. Mater. Sci. Mater. Med.* **2002**, *13*, 695–700. [CrossRef] [PubMed]
37. Bertrand, E.; Gloriant, T.; Gordin, D.M.; Vasilescu, E.; Drob, P.; Vasilescu, C.; Drob, S.I. Synthesis and characterisation of a new superelastic Ti–25Ta–25Nb biomedical alloy. *J. Mech. Behav. Biomed. Mater.* **2010**, *3*, 559–564. [CrossRef]
38. Zhang, D.C.; Mao, Y.F.; Li, Y.L.; Li, J.J.; Yuan, M.; Lin, J.G. Effect of ternary alloying elements on microstructure and superelastictity of Ti–Nb alloys. *Mater. Sci. Eng. A* **2013**, *559*, 706–710. [CrossRef]